Supporting Information

Unveiling Interface Interaction Assisted Broadband Photoresponse of Epitaxial 2D Bi_2O_2Se on Perovskite Oxides

Yujie Guo,[a] Yekai Song,[bcd] Manli Yang,[a] Zhenyu Xu,[a] Haowei Xie,[a] Hui Li,[e] Zhuojun Li,[*bc] Huawei Liang,[*a] Shuangchen Ruan,[a] and Yu-Jia Zeng[*a]

a. Key Laboratory of Optoelectronic Devices and Systems, College of Physics and Optoelectronic Engineering, Shenzhen University, Shenzhen, 518060, P. R. China. E-mail: yjzeng@szu.edu.cn, hwliang@szu.edu.cn

b. State Key Laboratory of Functional Materials for Informatics, Shanghai Institute of Microsystem and Information Technology, Chinese Academy of Sciences, Shanghai, 200050, P. R. China. E-mail: lizhuojun@mail.sim.ac.cn

c. CAS Center for Excellence in Superconducting Electronics (CENSE), Shanghai 200050, P. R. China

d. School of Physical Science and Technology, ShanghaiTech University, Shanghai 200031, P.R.China

e. College of Engineering Physics, Shenzhen Technology University, Shenzhen 518118, P. R. China

1. Dimension of the Bi_2O_2Se layer and laser powers

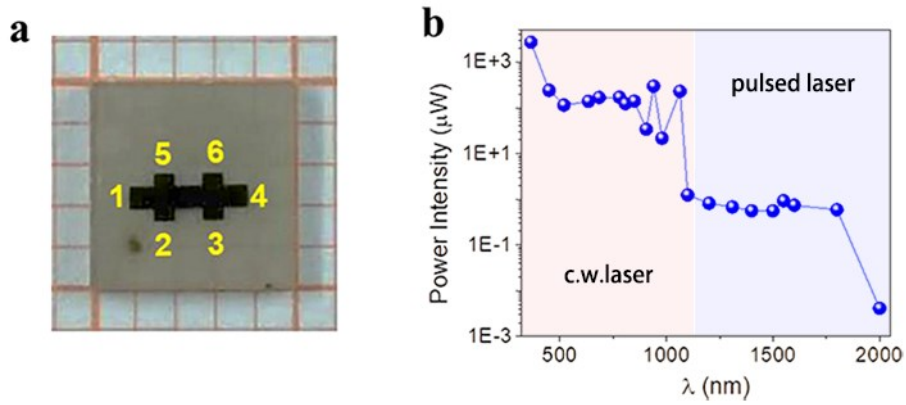

Fig. S1. (a) A photo of an as-grown Bi_2O_2Se layer on the $SrTiO_3$ (100) substrate, whose dimension is 0.5mm×3mm;1 (b) laser power intensity radiated on the devices PD.I-III (P) as a function of laser wavelength (λ). It is worth mentioning that the comparison of photoresponse properties among PD.I-III can only be done under the radiation of the same λ, as the laser power is λ dependent.

2. Figures of merit as a function of λ

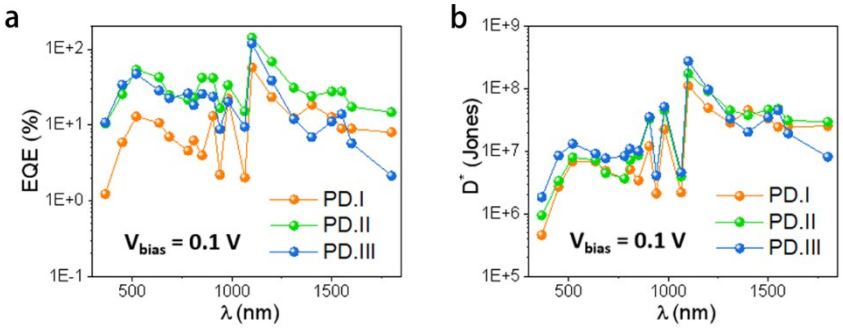

Fig. S2. (a) External quantum efficiency (EQE) and (b) detectivity (D^*) of PD.I-PD.III as a function of λ under 0.1 V external bias.

3. I_{ph} as a function of power intensity (P)

P of the pulsed lasers (wavelength range of 1100-1850 nm) was tuned to monitor the fluctuation of the photocurrent (I_{ph}). As plotted in Fig. S3, all I_{ph} measured from PD.I are fitted nicely to $I_{ph} \propto P^{\alpha}$ with α values from 0.155 to 1.007, whereas the device is photoconductive or photogating predominant when α = 1 or α = 0, respectively.[2–5] These data hint the co-existence of above-mentioned two effects in PD.I, and similar results were obtained in PD.II and III.

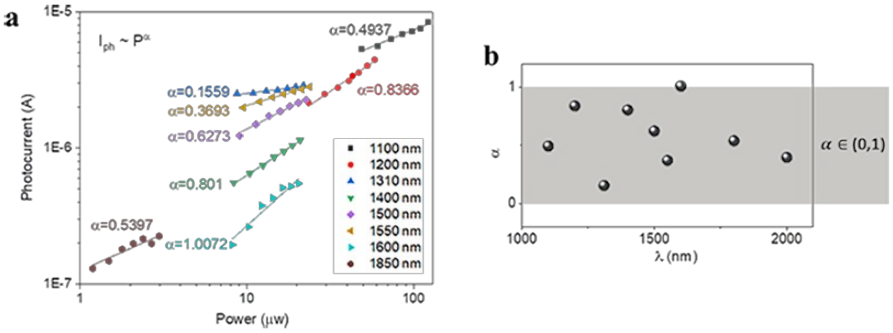

Fig. S3. (a) photocurrent (I_{ph}) as a function of P in PD.I; the dots represent the experimental data whereas lines refer to the nice fitting of $I \sim P^{\alpha}$; (b) plot of α values mostly in range from 0 to 1, representing the interplay of photoconductive and photogating effects.

4. Responsivity R as a function of P

Fig. S4 plots the R~P relationships in PD.I upon the pulsed-laser radiation. These curves are mainly linear yet in some cases approach the plateau at higher P, which are typically ascribed to the co-existence of thermal-induced mechanisms.

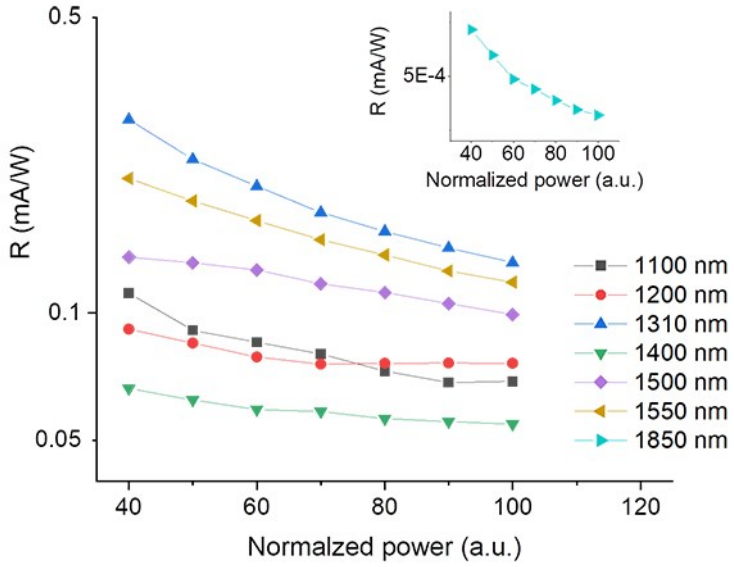

Fig. S4. Plot of resbonsivity (R) versus P, showing a general decline of R with the increase of P; in some cases, for instance radiant by 1100nm, 1200nm and 1850nm, the slops of lines gradually decrease with the increase of P, indicating the enrolment of thermal-correlated effects in the photodetector

5. Pyroelectric photoresponse under the visible light radiation or in the Bi_2O_2Se/Si photodetector

Fig.5a plots an example of the unconventionally low pyroelectric photoresponse under visible light radiation owing to the large channel area and planar electrodes' configuration. The photoresponse of the Bi_2O_2Se/Si photodetector is shown in Figure 5b, in which the measured I-t curve yields only one instant current peak right after switching on the laser. We therefore deduce that Bi_2O_2Se and $SrTiO_3$ are both obligated to the pyroelectricity in the $Bi_2O_2Se/SrTiO_3$ photodetectors.

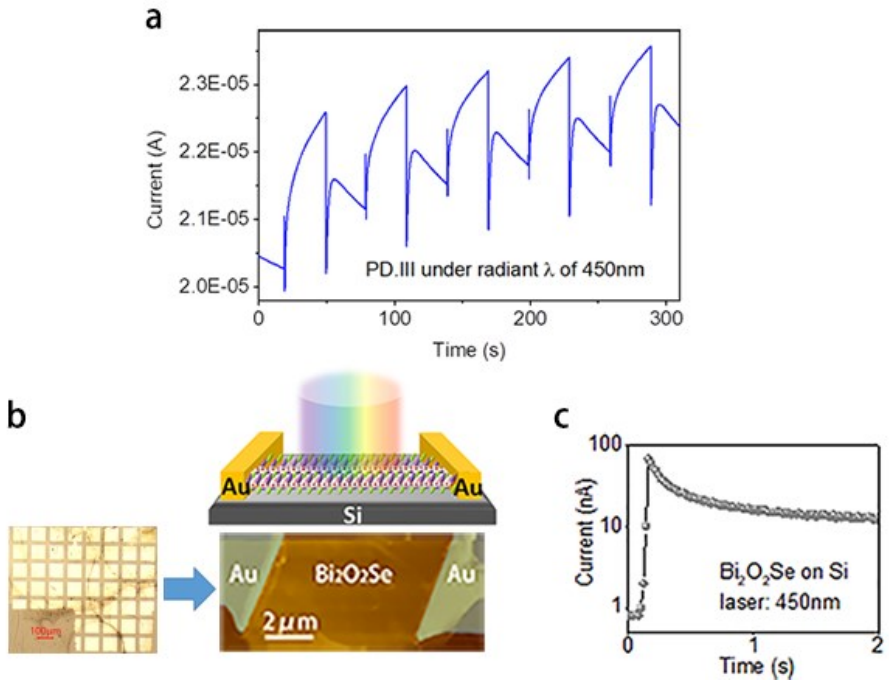

Fig. S5. (a) I-t curve of PD.III illuminated by the 450 nm laser showing lower pyroelectric current than the corresponding saturated photocurrent. (b) top: a schematic of the Bi_2O_2Se/Si device; bottom: an optical microscope image of the selectively etched as-grown Bi_2O_2Se layer before transferring; an AFM image of the Bi_2O_2Se/Si photodetector; (c) I-t curve of the device under the illumination of 450 nm laser.

6. I-V curves of PD.II' and PD. III'

The shift of the I-V curves with respect to the origin is observed when illuminated at two ends. The shifting direction follows the contact polarity, in consistent with the scenario shown in Figure 5b at zero bias.

It is noteworthy that the "center" positions in I-V curves of PD I'-III' (Figure S6) have a different meaning from the one defined in the I-t curves in Figure 5b. The former refers to the position with zero internal potential, by which means, the position of zero net current under laser radiation and zero bias. The latter is defined by the geometric centre of the device. In PD.I'-III' these two "centre" positions do not overlap, elucidating slightly asymmetric work functions at two ends. This result is in consonance with the observation showing unequal absolute current values at two ends.

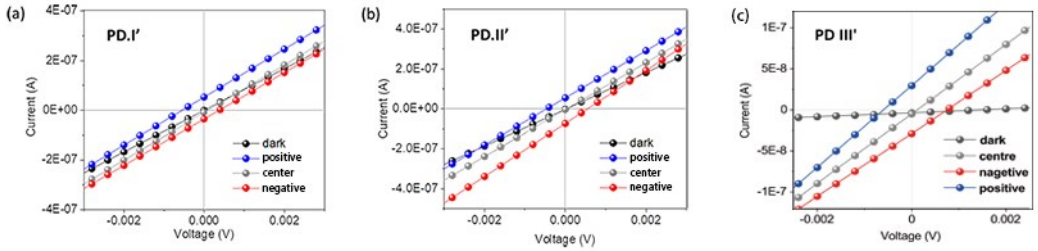

Fig. S6. I-V curves around the origin points measured in (a) PD. I', (b) PD. II' and (c) PD. III' where I-V curves are measured at two ends and in the channel centre.

7. Thickness dependent photoresponse under zero bias

The self-powered photoresponse is not highly seebeck coefficient (S) dependent. Based on the semiclassical Boltzmann transport theory, a trade-off between S and carrier concentration (n) can be expressed:[6,7]

$$S = \frac{8\pi^2 k_B^2}{3eh^2} m^* T \left(\frac{\pi}{3n}\right)^{2/3} \quad (4)$$

where k_B and m^* are the Boltzmann constant and the electron effective mass, respectively. Hence, owing to the positive correlation between δ and n in our PLD-grown Bi_2O_2Se layers, S varies inversely to δ.[1] Thereby, S is excluded from the predominant impact on the photoresponse.

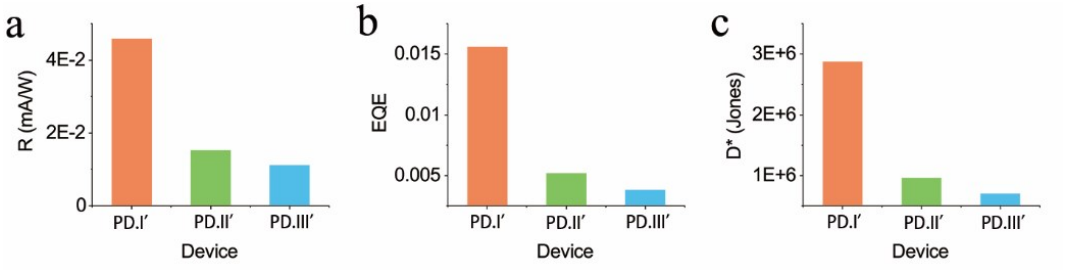

Fig. S7. Self-powering photoresponse. Comparison of (a) R; (b) external quantum efficiency (EQE); (c) detectivity (D*) among PD.I'-III' under zero bias

.

8. Table S1: performance comparison of Bi_2O_2Se-based photodetectors under external bias of 1V

Substrate	gating	Lateral dimension (μm)	Detection band (nm)	R(A/W)	D* (Jones)	Detected wavelength (nm)	Ref.
$SrTiO_3$	No	500	365-1850	12.62	1.51×10^9	1100	This work
Mica	No	100	350-1600	320	-	550	8
Mica	No	10	360-1090	9.1	1.3×10^8	640	3
Mica	No	7-11	808	6.5	8.3×10^{11}	808	9
Mica	Yes		360-1800	108 696	8.2×10^{12}	360	10
Si	Yes	5		3.5×10^4	9×10^{13}	532	4

Under the optimal condition of Bi_2O_2Se transferring, a much better photoresponse can be achieved owing to the scaled channel dimension and external gating. Nevertheless, the manufacturing of photodetectors based on the as-grown Bi_2O_2Se photodetectors is facile that skips the complicated procedures of transferring Bi_2O_2Se to the Si substrate. In addition, it impedes the contamination and quality degradation of the crystal during transferring.

References

1 Y. Song, Z. Li, H. Li, S. Tang, G. Mu, L. Xu, W. Peng, D. Shen, Y. Chen, X. Xie and M. Jiang, *Nanotechnology*, 2020, **31**, 165704.

2 P. Luo, F. Zhuge, F. Wang, L. Lian, K. Liu, J. Zhang and T. Zhai, *ACS Nano*, 2019, **13**, 9028–9037.

3 X. Liu, R. Li, C. Hong, G. Huang, D. Pan, Z. Ni, Y. Huang, X. Ren, Y. Cheng and W. Huang, *Nanoscale*, 2019, **11**, 20707–20714.

4 Q. Fu, C. Zhu, X. Zhao, X. Wang, A. Chaturvedi, C. Zhu, X. Wang, Q. Zeng, J. Zhou, F. Liu, B. K. Tay, H. Zhang, S. J. Pennycook and Z. Liu, *Adv. Mater.*, 2019, **31**, 1804945.

5 B. Deka Boruah, S. Naidu Majji, S. Nandi and A. Misra, *Nanoscale*, 2018, **10**, 3451–3459.

6 L. Pan, L. Zhao, X. Zhang, C. Chen, P. Yao, C. Jiang, X. Shen, Y. Lyu, C. Lu, L.-D. Zhao and Y. Wang, *ACS Appl. Mater. Interfaces*, 2019, **11**, 21603–21609.

7 Y. Wang, Y. Niu, M. Chen, J. Wen, W. Wu, Y. Jin, D. Wu and Z. Zhao, *ACS Photonics*, 2019, **6**, 895–903.

8 H. Yang, C. Tan, C. Deng, R. Zhang, X. Zheng, X. Zhang, Y. Hu, X. Guo, G. Wang, T. Jiang, Y. Zhang, G. Peng, H. Peng, X. Zhang and S. Qin, *Small*, 2019, 1904482.

9 J. Li, Z. Wang, Y. Wen, J. Chu, L. Yin, R. Cheng, L. Lei, P. He, C. Jiang, L. Feng and J. He, *Adv. Funct. Mater.*, 2018, **28**, 1–7.

10 T. Tong, Y. Chen, S. Qin, W. Li, J. Zhang, C. Zhu, C. Zhang, X. Yuan, X. Chen, Z. Nie, X. Wang, W. Hu, F. Wang, W. Liu, P. Wang, X. Wang, R. Zhang and Y. Xu, *Adv. Funct. Mater.*, 2019, 1905806.